OPEN ACCESS
IOP Publishing
Measurement Science and Technology
Meas. Sci. Technol. **32** (2021) 125202 (12pp)
https://doi.org/10.1088/1361-6501/ac1dfa

Correction of periodic displacement non-linearities by two-wavelength interferometry

Angus Bridges[1,2], **Andrew Yacoot**[1,2], **Thomas Kissinger**[2], **David A Humphreys**[1,3] and **Ralph P Tatam**[2,*]

[1] National Physical Laboratory, Teddington, Middlesex TW11 0LW, United Kingdom
[2] Centre for Engineering Photonics, Cranfield University, Cranfield MK43 0AL, United Kingdom
[3] Department of Electrical and Electronic Engineering, University of Bristol, Bristol BS8 1UB, United Kingdom

E-mail: r.p.tatam@cranfield.ac.uk

Received 24 May 2021, revised 27 July 2021
Accepted for publication 16 August 2021
Published 31 August 2021

Abstract

Non-linearities in interferometric displacement measurements commonly affect both homodyne and heterodyne optical interferometers. Unwanted back reflections (ghost reflections) or polarisation leakage introduce non-linearity terms at harmonics of the illuminating wavelength that cannot be fully corrected for with standard non-linearity correction techniques. A two-wavelength interferometric approach, operating at 632.8 and 785 nm, is presented here that is capable of correcting such non-linearities. Non-linearities are separated from the difference between two displacement measurements made at differing wavelengths with a Fourier approach. Compared to a standard Heydemann ellipse fitting correction, the proposed approach reduces estimated residual non-linearities from 84 to 11 pm in the case of a linear displacement profile. In particular this approach is applicable to the correction of higher order non-linearities that are caused by multiple reflections, and that are therefore very sensitive to alignment conditions.

Keywords: interferometry, non-linearity, dimensional metrology

(Some figures may appear in colour only in the online journal)

1. Introduction

Non-linearities, defined here as errors in the interferometric measurement of displacement that are periodic with harmonics of the operating wavelength, affect almost all interferometric displacement measurements [1]. Whilst in longer range applications these errors, typically ranging from picometres to nanometres in magnitude, may be insignificant in comparison to refractive index or optical frequency uncertainties [2], for displacements made over smaller length scales, or in more tightly controlled environments, non-linearities can be the ultimate limit for the achievable measurement uncertainty [3]. Although picometre level non-linearities have been achieved with complex interferometer designs [4], these very low non-linearities may be dependant on the exact alignment, or misalignment, of the interferometer optics, and as such may not be transferable between separate instruments, and cannot be guaranteed in practice without comparison to a more linear displacement standard [3].

Unwanted cavity formation within interferometer optics, either due to polarisation leakage or unwanted back reflections (ghost reflections) has been identified as a source of non-linearities in a number of homodyne and heterodyne interferometer designs [5–11]. Whilst analyses of such non-linearity sources have been made [6–8, 10, 12, 13], and in some cases

* Author to whom any correspondence should be addressed.

the effects of these non-linearities can be reduced through improved optical design or alignment [8, 14, 15], complete elimination is often impossible. As a result, residual non-linearity errors that are highly dependant on the exact alignment of the interferometer optics, and that range from tens to hundreds of picometres in magnitude, may remain in interferometer systems

A wide range of non-linearity correction algorithms have been proposed in the literature, many following the ellipse fitting technique developed by Heydemann [16] for ultrasonic instruments, and first applied to optical interferometry by Birch [17]. This correction, applicable to both homodyne [17] and heterodyne [18] interferometers, aims to compensate for errors in interferometers that output quadrature signals by adjusting the quadrature phase difference between the signals along with the relative gains and zero offsets by transforming an elliptical Lissajous figure to the ideal circular form. Improvements to the Heydemann correction have been proposed, applying differing ellipse fitting algorithms to the problem [19–23], however all are ultimately limited to the correction of elliptical non-linearities, defined as periodic errors that distort the Lissajous figure to an elliptical form, and as such are unable to correct for higher order non-linearities that result in a non-elliptical Lissajous figure [10, 13].

Alternative non-linearity correction methodologies aiming to compensate only for quadrature phase differences, relative gains and offsets have also been proposed based on peak detection [24] and identification of low error points on the ellipse [25]. These approaches allow certain non-linearities to be corrected for in real time, but are also limited to the correction of elliptical non-linearities.

One correction approach has been proposed in the literature [26] that is capable of the correction of non-elliptical non-linearities, based upon fitting a sum of sinusoidal non-linearity harmonics with variable phase and amplitude to the difference between a measured interferometric displacement and the same displacement measured with a capacitance sensor. This approach is limited to applications in which attaching a capacitance sensor to the target to be measured is possible, and to displacement ranges suitable for capacitive measurement, although the authors do suggest alternative secondary displacement measures. In addition to this, fixed amplitude and phase non-linearity terms are fitted in [26]. Higher order non-linearity terms are highly sensitive to the optical alignment, and therefore may vary with both displacement and time, limiting the performance of the capacitive correction where non-linearities vary on a fringe to fringe basis.

Two-wavelength interferometer designs have previously been developed for refractive index compensation [27–29], absolute length measurement [30], and non-linearity evaluation [4, 31]. The possibility of exploiting the periodic nature of non-linearity errors to evaluate residual non-linearities, by observing the magnitude of the difference between displacement measurements made at two wavelengths has previously been recognised [4, 31], however, the correction of non-linearities through two-wavelength interferometry has not previously been demonstrated.

In the work presented here a non-linearity correction algorithm is proposed, implemented as a post-processing technique, that makes use of two coaxial optical interferometers operating along the same beam path but at differing wavelengths. The difference between the measured displacements is calculated, and, through Fourier analysis, non-linearity terms at spatial harmonics of each wavelength are separated. The non-linearity errors in each interferometer are then subtracted from the measured displacements, resulting in a corrected displacement measurement. In contrast to the commonly employed Heydemann style ellipse fitting correction, this technique allows for the correction of higher order non-linearity terms that produce non-sinusoidal quadrature signals and non-elliptical Lissajous figures. In this paper the basic principle of the proposed correction algorithm is outlined, followed by a discussion of the data processing techniques required to minimise edge effects and spectral leakage arising from the Fourier approach. The correction algorithm is then demonstrated in a proof of concept experiment for a variety of displacement profiles. As this is a proof of concept work, potential improvements to the technique and required future work are discussed.

2. Theory and data processing methods

In order to describe the two-wavelength non-linearity correction methodology, a basic introduction to the principles of the technique will first be given, followed by a discussion of the limits of the Fourier approach and the data processing techniques required to mitigate these limits.

2.1. Principles of the two-wavelength non-linearity correction

Defining non-linearities as errors in the measured interferometric displacement that are periodic with harmonics of the illuminating wavelength, and neglecting all other error sources, the measured interferometric displacement at a wavelength λ_a may be written as:

$$x_a = x + \sum_{j=1}^{j_{max}} A_{a,j} \cos\left(4\pi \frac{j}{\lambda_a} x + \phi_{a,j}\right), \tag{1}$$

where x is the true displacement and $A_{a,j}$ and $\phi_{a,j}$ are amplitude and phase coefficients at the j^{th} harmonic respectively. An optical configuration resulting in only even harmonics being present in the measured displacement is assumed in this work. This is the case for the majority of displacement measuring interferometer designs, which operate almost universally in a two or four pass configuration, with one optical fringe corresponding to one half or one quarter of the illuminating wavelength in displacement.

The true displacement x cannot in general be recovered from x_a, as, although the error is known to be periodic, it is periodic with x, which is unknown. x could be recovered from x_a if the sample spacing was known to be uniform in x, however uniform sample spacing would require a constant velocity, and therefore severely limit the applicability of the technique.

In this two-wavelength interferometry technique displacement is measured simultaneously with two interferometers operating at different wavelengths along a common beam path. A second displacement measurement is therefore introduced, given by:

$$x_{\mathrm{b}} = x + \sum_{j=1}^{j_{\max}} A_{\mathrm{b,j}} \cos\left(4\pi \frac{j}{\lambda_{\mathrm{b}}} x + \phi_{\mathrm{b,j}}\right). \tag{2}$$

The shortest spatial period harmonic that can be resolved will be determined in the case of uniform sample spacing by the Nyquist frequency, and will therefore be given, for a sample spacing Δx, by:

$$j_{\max} = \left\lfloor \frac{\min(\lambda_{\mathrm{a}}, \lambda_{\mathrm{b}})}{4\Delta x} \right\rfloor. \tag{3}$$

Higher order harmonics will tend to be strongly attenuated by losses and minor misalignments within the interferometer optics, and as a result of this in many cases $j_{\max}$ will be limited by the optical design of the interferometer, rather than the spatial sampling rate. Typically harmonics of up to four times the fringe period of the interferometer are observed.

The basic principles of the non-linearity correction methodology are shown in figure 1, with figures 1(A) and (B) showing x_a and x_b as defined in equations (1) and (2). Comparing equations (1) and (2), it can be seen that if the harmonic coefficients $A_{\mathrm{a/b,j}}$ or $\phi_{\mathrm{a/b,j}}$ can be determined, the true displacement can be recovered from the displacement measurement at either wavelength. Taking the difference between the two displacement measurements yields a combined sum over both sets of harmonics as:

$$d = x_{\mathrm{a}} - x_{\mathrm{b}}, \tag{4}$$

$$= \sum_{j=1}^{j_{\max}} \left(A_{\mathrm{a,j}} \cos\left(4\pi \frac{j}{\lambda_{\mathrm{a}}} x + \phi_{\mathrm{a,j}}\right) - A_{\mathrm{b,j}} \cos\left(4\pi \frac{j}{\lambda_{\mathrm{b}}} x + \phi_{\mathrm{b,j}}\right)\right), \tag{5}$$

shown in figure 1(C).

The problem then becomes one of separating harmonics of differing spatial periods, pointing naturally towards a Fourier approach. The amplitudes of the discrete Fourier transform (DFT) of the displacement difference are presented in figure 1(D), where in order to separate the non-linearity harmonics a rectangular window function has been applied around the first three even harmonics of λ_{a}, in this case corresponding to spatial periods of 316.5, 158.25 and 105.5 nm. The width of the window around each non-linearity harmonic is set in this work to twice the frequency resolution of the DFT. Having applied this window function, the DFT is then inverted, resulting in an estimate of the non-linearity error in the measured displacement x_{a}, shown in figure 1(E), that approximates the non-linearity error as:

$$e_{\mathrm{a}} \approx \sum_{j=1}^{j_{\max}} A_{\mathrm{a,j}} \cos\left(2\pi \frac{j}{\lambda_{\mathrm{a}}} x + \phi_{\mathrm{a,j}}\right). \tag{6}$$

This error estimate is then subtracted from the measured displacement, resulting in a displacement measurement with reduced non-linearities, given by:

$$x_{\mathrm{a,c}} = x_{\mathrm{a}} - e_{\mathrm{a}}, \tag{7}$$

as shown in figure 1(F). Whilst in this example the correction has been applied to x_{a} only, the same approach may also be applied to x_{b}.

The spatial period windowing approach adopted here restricts this technique to cases where the non-linearity harmonics do not overlap, a condition that is dependant on the choices of λ_{a} and λ_{b}, the displacement range covered, and the stability of the non-linearities. Assuming uniform spatial sampling, ideally stable wavelengths, and non-linearities that remain stable in both amplitude and phase throughout the measurement such that no peak broadening takes place, the frequency spacing between non-linearity terms must remain greater than the frequency resolution of the DFT, given by the inverse of the displacement range covered. In this work, wavelengths of 632.8 and 785 nm were adopted, with the first closely spaced spatial harmonics occurring at 79.1 nm (the 8th harmonic of 632.8 nm) and 78.5 nm (the 10th harmonic of 785 nm). Separating these harmonics under ideal conditions would require a displacement range of 10.3 μm, with a sample spacing of less than 39.25 nm. As previously discussed, higher order harmonics are likely to be strongly attenuated by the interferometer optics, and as such this restriction is not anticipated to limit the performance of the correction. If the harmonics present in the interferometer outputs are known, λ_{a} and λ_{b} may be chosen to avoid overlaps.

2.2. Spatial resampling

For a (spatially) uniformly sampled displacement measurement, the described approach may prove sufficient, however many real world measurements will not be uniformly spatially sampled due to non-linear displacement paths. Further problems arise with the methodology proposed in figure 1 due to the finite sample length and non-integer number of periods contained in the sample. The results of this are apparent in figure 1(D) where the amplitude peaks in the DFT are broadened, and in figures 1(E) and (F) as a low frequency modulation in the estimated non-linearity error amplitude where none exists in the modelled data. In addition to these problems, the measured displacement, either x_{a} or x_{b}, chosen to form the 'timebase' of the DFT contains the non-linearity errors, and the effects of this timebase modulation must be considered.

To counter first the problem of non-uniform sampling, the calculated displacement differences d must be interpolated onto a linear displacement basis, resulting in:

$$d_{\mathrm{a,L}} = \sum_{j=1}^{j_{\max}} \left(A'_{\mathrm{a,j}} \cos\left(4\pi \frac{j}{\lambda_{\mathrm{a}}} x_{\mathrm{a,L}} + \phi'_{\mathrm{a,j}}\right) - A'_{\mathrm{b,j}} \cos\left(4\pi \frac{j}{\lambda_{\mathrm{b}}} x_{\mathrm{a,L}} + \phi'_{\mathrm{b,j}}\right)\right), \tag{8}$$

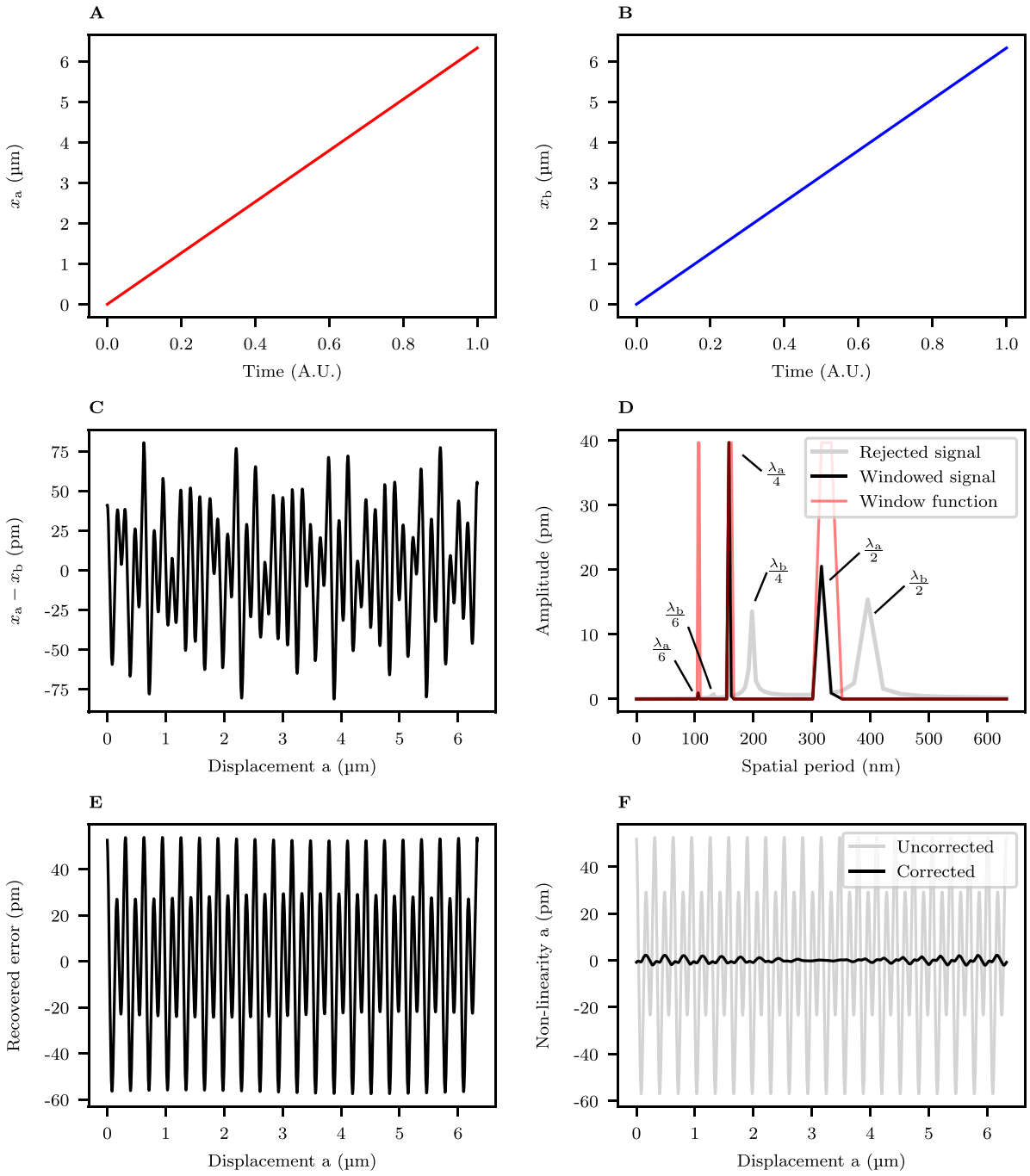

Figure 1. Basic principles of the two-wavelength non-linearity correction methodology, illustrated here for the simple case of a linear movement, as applied to modelled data for $\lambda_a = 633$ nm and $\lambda_b = 785$ nm. (A) Displacement is measured with interferometer 'a', operating at λ_a. (B) Displacement is measured simultaneously with interferometer 'b', operating at λ_b. (C) Difference between the 'a' and 'b' displacements is calculated. (D) Fourier transform is applied to the displacement difference and windowed around spatial harmonics of λ_a. (E) Estimated non-linearity errors in the λ_a displacement are recovered by inverting the windowed Fourier transform of the displacement difference. (F) Estimated non-linearity errors are subtracted from displacement a, resulting in a displacement measurement with reduced non-linearity. Edge effects are visible, resulting from a non-integer number of periods being included in the Fourier transform.

and

$$d_{b,L} = \sum_{j=1}^{j_{max}} \left(A'_{a,j} \cos\left(4\pi \frac{j}{\lambda_a} x_{b,L} + \phi'_{a,j}\right) - A'_{b,j} \cos\left(4\pi \frac{j}{\lambda_b} x_{b,L} + \phi'_{b,j}\right)\right), \quad (9)$$

for interpolations carried out with respect to the x_a and x_b measurements respectively, where $x_{a,L}$ and $x_{b,L}$ are the linearly spaced displacements and the primed amplitude and phase coefficients indicate that these coefficients are not identical to those in equation (4) due to the aforementioned timebase modulation. A nearest neighbour interpolation algorithm is applied

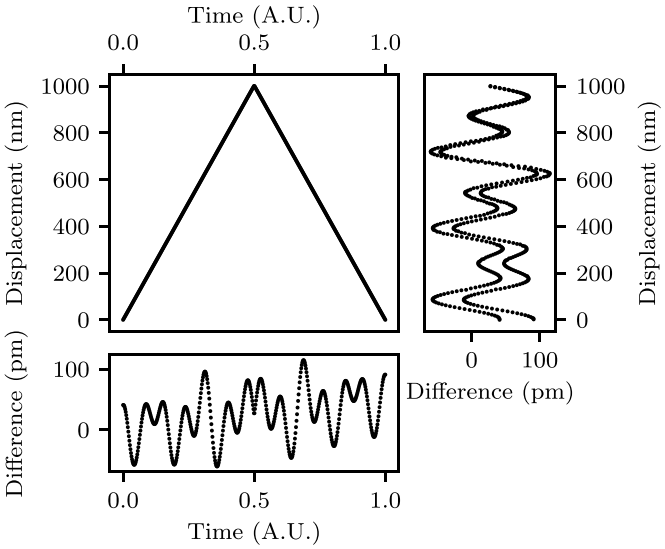

Figure 2. Demonstration of the effect of multiple displacement values at each displacement point on the interpolation process for a measurement including a linear 50 pm drift over the full measurement period between the λ_a and λ_b displacement measurements.

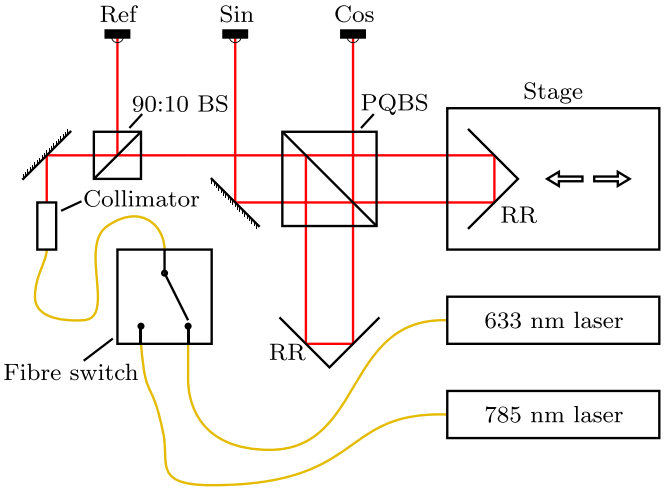

Figure 3. Schematic of the two-wavelength interferometer. RR, retro-reflector; PQBS, phase-quadrature beam splitter; 90:10 BS, reference pick off beam splitter; Ref, intensity reference photodiode; Sin, sine quadrature photodiode; Cos, cosine quadrature photodiode.

here, chosen to avoid biasing the results with an interpolation algorithm more closely matched to the physical displacements generated in the experimental work. In the case of displacement profiles that are self-overlapping, this interpolation process will, in the case of nearest neighbour interpolation, introduce some high frequency fluctuations between the multiple displacement values if drift between the two interferometers occurs, as demonstrated in figure 2. These high frequency fluctuations will be filtered out by the Fourier transform and windowing process, and as such will not affect the corrected displacement.

The effects of a non-integer number of periods within the finite sample length are mitigated by first clipping $d_{a,L}$ and $d_{b,L}$ to an integer number of fringes for each wavelength respectively, then tiling the clipped data onto the start and end of the data set. Separate interpolations of the displacement difference are carried out for the x_a and x_b displacements as due to the periodicity of the non-linearities, the errors due to the non-linearities at harmonics of each wavelength are zero at multiples of that wavelength. The use of separate interpolations therefore allows the data to be clipped to an integer number of fringes as precisely as possible for each wavelength. For the experimental results gathered here this approach was found to be successful, however, it should be noted that by tiling the data the implicit assumption is made that non-linearity errors at the start and end of the displacement range are similar. Displacement differences falling outside of an integer number of fringes are therefore, as a consequence of the tiling, corrected based on the errors at the opposite end of the integer fringe range. This extrapolation is only appropriate where the previously stated assumption holds.

Following the frequency space windowing and DFT inversion the recovered non-linearity estimates $e_{a,L}$ and $e_{b,L}$ must then be interpolated back onto the measured displacements x_a and x_b before subtracting to give the corrected measurements. In this work a nearest neighbour interpolation approach was once again used for the back interpolation step.

3. Experimental methods

In order to demonstrate the two-wavelength non-linearity methodology experimentally, a homodyne Michelson interferometer was constructed making use of a phase-quadrature beam splitter (PQBS) [32] cube designed originally for use at 633 nm. A schematic of the interferometer is shown in figure 3. The external faces of the PQBS and the front surfaces of the solid glass corner cube retroreflectors were deliberately aligned to introduce higher order non-linearities. λ_a was provided by a thermally stabilised helium-neon (HeNe) laser operating at approximately 632.8 nm (REO 32 734) and λ_b was provided by a 785 nm diode laser (Schäfter + Kirchhoff 51nano-S-785-12-Q06-P-5-2-18-0-150). The two wavelengths were multiplexed together with a MEMS fibre optic switch (Sercalo SN-1x2-4-N) using a switching frequency of approximately 30 Hz. By fibre coupling both laser sources into the same fibre, coaxial propagation of the two interferometers is ensured. A mirror collimator was employed to ensure beams at both wavelengths were collimated. ThorLabs SM600 fibre was used from the fibre switch to the collimator, with a cut off wavelength between 500 and 600 nm. At a wavelength of 785 nm this fibre may exhibit some undesirable bend losses; the effect of any varying losses were minimised by normalisation to an intensity reference output. The reference, sine and cosine photodiode outputs shown in figure 3 were amplified and digitised simultaneously with electronics developed in house at the National Physical Laboratory (NPL). Demultiplexing of the two wavelengths was carried out in software based on rising edges in the reference channel signal, with the sine and cosine channels normalised relative to the

demultiplexed reference for each wavelength in order to minimise the effects of longer term drift in the laser powers. A further normalisation based upon a Gaussian envelope fitted to maxima and minima of the sine and cosine fringes was carried out for the λ_b fringes. This normalisation was required to compensate for the low coherence length (approximately 300 μm) of the 785 nm laser.

A Heydemann correction [16, 17] was applied to both sets of fringes prior to applying the two-wavelength correction. The Heydemann correction fits an ellipse to the Lissajous figure formed by plotting the two quadrature outputs of a homodyne interferometer against each other, and uses the resulting ellipse fit coefficients to transform the Lissajous figure to the ideal origin centred circular form. As a result, any quadrature phase errors, signal offsets and gain ratio errors are minimised.

Whilst applying the Heydemann correction in this case was not strictly necessary, as the two-wavelength correction may also be employed to correct for the effects of elliptical distortions to the quadrature signals, some offset must be applied to the measured optical powers in order to ensure the origin falls within the approximately elliptical Lissajous figure, in order to allow fringe counting to take place. As the Heydemann correction has no disadvantages in this case, with the restrictions to displacements of greater than one optical fringe and non-real time correction shared with the two-wavelength approach, the Heydemann correction was employed as a pre-processing step.

The interferometric phase was then calculated through a four-quadrant arctangent function, and unwrapped at discontinuities of greater than π. For this proof of concept experiment no environmental parameters were recorded, and therefore no Edlén style wavelength corrections [33] were applied and the laser wavelengths were assumed constant. The small scaling errors introduced by this assumption do no affect the ability of the system to distinguish the presence of non-linearity harmonics, and any error in the estimated amplitude of the non-linearity harmonics introduced by this fixed wavelength assumption is estimated to be less than 1 pm. As no wavelength changes were measured, and the interferometer was operated with a path length difference of the order of micrometres, displacements for the λ_a interferometer were calculated without a dead path correction term [34] as:

$$x_a = \frac{\lambda_a}{4\pi}\varphi_a, \tag{10}$$

where φ_a is the unwrapped interferometric phase for the λ_a interferometer, based on a wavelength of 632.8 nm. λ_b displacements were calculated from the unwrapped interferometric phase at λ_b, φ_b, as:

$$x_b = \frac{\max(x_a) - \min(x_a)}{\max(\varphi_b) - \min(\varphi_b)}\varphi_b, \tag{11}$$

negating any requirement for precise knowledge of the wavelength λ_b.

Test displacements were generated with a Queensgate Instruments NPS-X15A nanopositioning stage, and non-linearities before and after correction were estimated from a DFT of the displacement error relative to the stage position, permitting non-linearities to be separated from higher frequency noise and lower frequency drift terms.

This system, whilst non-optimal for precision interferometry, proved sufficient to serve as a proof of concept of the two-wavelength methodology. The limitations of this system are considered in the discussion section, along with suggested improvements for a system suitable for practical application.

Three displacement scan profiles were used to demonstrate the two-wavelength correction: a unidirectional linear scan, a mirrored linear scan and a sinusoidal scan, as shown in figures 4(A–C). In all cases the stage was moved in 1000 steps through a 15 μm range, allowing both the effects of non-uniform spacing (in the case of the sinusoidal scan) and multiple displacement difference values at each displacement point (in the case of the mirrored linear scan) to be tested.

4. Results

Considering first the linear displacement profile (figure 4(A)), the calculated displacement difference between the two interferometers at each stage position in shown in figure 4(D). Due to the relatively large amount of drift between the interferometers, introduced by a combination of drift in λ_b, refractive index fluctuations and thermal fluctuations over the course of the measurement, non-linearities are not clearly visible. The combined effects of refractive index fluctuations (including dispersion between the two wavelengths) and thermal drifts can also be seen in figures 4(E, F, J, K and L). These effects are non-repeatable. The DFT of the interpolated displacement differences is shown for the linear displacement profile in figure 4(G), with peaks apparent at spatial periods of $\lambda_a/2$, $\lambda_a/4$ and $\lambda_a/6$. Figure 4(J) shows the results of the correction made based upon the windowed DFT shown in figure 4(G), with displacement errors shown relative to the stage position for interferometric displacement measurements made at λ_a following the application of both a Heydemann correction, and a combined Heydemann and two-wavelength correction. DFTs of the λ_a displacement errors relative to the stage positions are shown for Heydemann corrected and Heydemann and two-wavelength corrected displacements in figure 4(M), with the estimated non-linearity amplitude, calculated as the sum of the $\lambda_a/2$, $\lambda_a/4$ and $\lambda_a/6$ DFT peaks, reduced from 84 to 11 pm.

Corresponding results are also shown in figure 4 for the mirrored linear displacement profile (B, E, H, K and N) and sinusoidal displacement profile (C, F, I, L and O). Non-linearities, again estimated as the sum of the first three even harmonics of λ_a, were reduced from 86 pm to 18 pm for the mirrored linear displacement profile. For the the sinusoidal displacement profile estimated non-linearities were reduced from 89 to 26 pm. It should be noted that as non-linearities were estimated with a Fourier technique, the estimates may be less accurate for the non-uniform mirrored linear and sinusoidal displacement profiles, as interpolation onto a linear displacement basis was required prior to applying the DFT. The increased magnitude of errors with spatial periods above

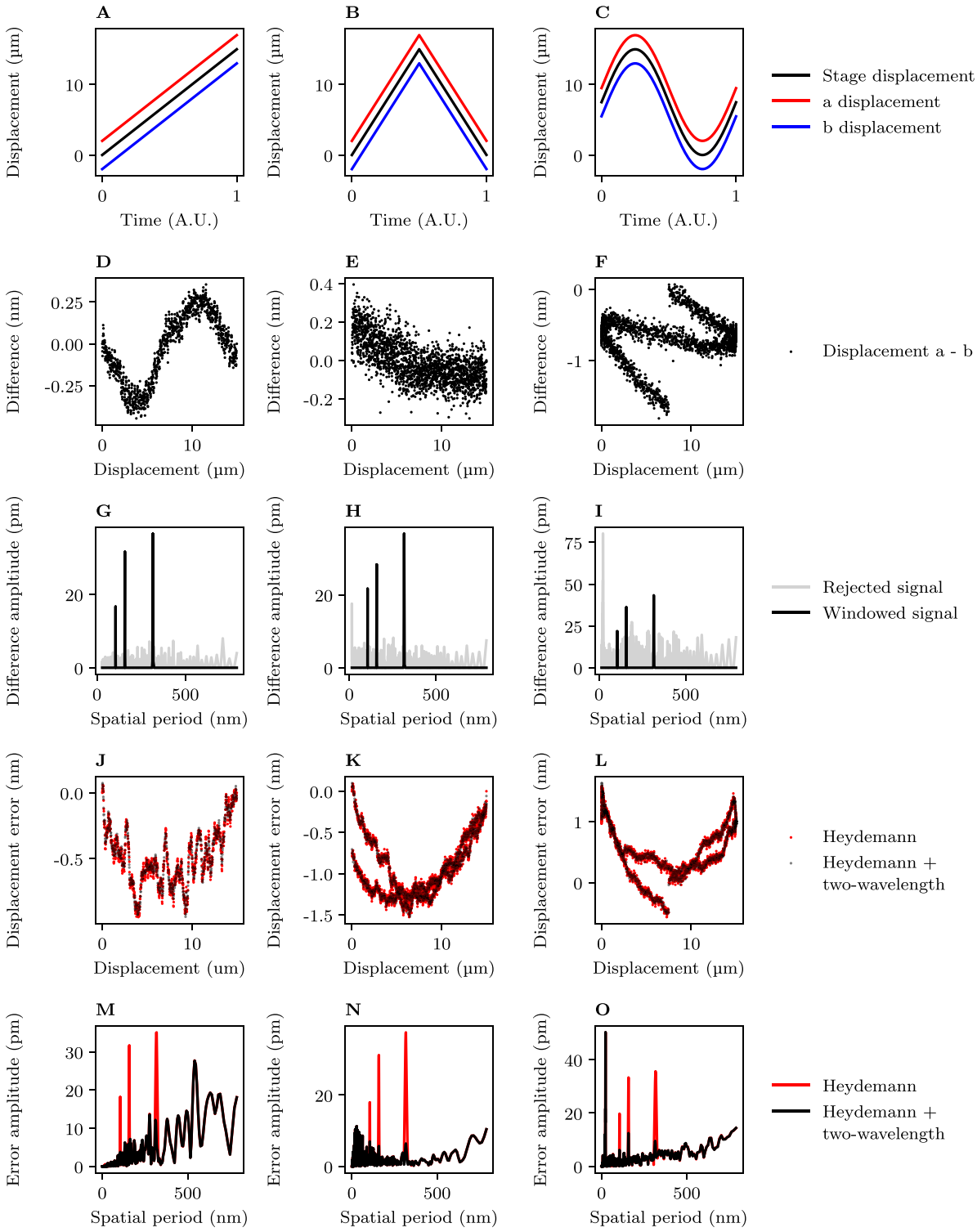

Figure 4. Stages of the two-wavelength non-linearity correction process for three displacement profiles (A, B and C) as applied to correction of the λ_a displacement measurement. Offsets have been applied to the displacement profiles in (A, B and C) for clarity. (D, E and F) Difference between the λ_a and λ_b interferometer displacement measurements. (G, H and I) DFT of the displacement difference following the interpolation, clipping and tiling process described in the text, with interpolation performed relative to the λ_a displacements. (J, K and L) Errors in the λ_a displacement measurements, relative to the stage position, for the three displacement profiles, and for both Heydemann corrected and Heydemann and two-wavelength corrected data. (M, N and O) DFTs of the data presented in (J, K and L), the error harmonics relative to the stage position, in contrast to error harmonics in the difference between the two interferometric displacement measurements, shown in (G, H and I).

300 nm present in figure 4(J) are responsible for the increased noise floor in figure 4(M) as compared to figures 4(N and O). These fluctuations are again attributed to air turbulence effects.

In order to investigate the effects of reduced displacement scan ranges on the correction, data from the linear displacement scan shown in figure 4 was taken in segments covering 100 displacement ranges of 1–7.5 μm with randomly generated offsets from the starting displacement in the range 0–7.5 μm applied. Non-linearity amplitudes in the λ_a interferometer were then estimated from the sum of the displacement error DFT peaks for the first three even harmonics. This process was repeated with 1000 randomly generated offsets, and means and standard errors in the means calculated, as plotted in figure 5. As may be expected from a Fourier technique the non-linearity correction can be seen to be more effective where a larger displacement range is available, however some non-linearity reduction remains possible down to a displacement range of 1 μm. Oscillations in the two-wavelength corrected non-linearity are introduced by the varying number of fringes contained in the displacement range. It should be noted that for smaller displacement ranges the Fourier estimation of non-linearity amplitudes becomes less reliable.

5. Discussion

The results presented here demonstrate the capability of the two-wavelength non-linearity correction methodology to improve upon the non-linearities achieved by application of the commonly employed Heydemann style [16, 17] ellipse fitting correction. In particular, non-linearities introduced by unwanted cavity formation within the optics, present in many interferometer designs due to back reflections (as is the case in this work) or polarisation leakage, may be corrected for with the two-wavelength methodology, a correction that to the knowledge of the authors has not previously been possible with a purely optical instrument. Additionally, the required precision of the ellipse fitting correction is reduced, as residual non-linearities after the ellipse fitting correction are corrected by the two-wavelength correction. Whilst a homodyne interferometer design has been demonstrated in this case, the technique is anticipated to be equally applicable to heterodyne systems.

Residual non-linearities have been estimated in this work using a Fourier technique. As such, there is some uncertainty associated with the residual non-linearity estimates. Non-linearities that vary with displacement may be underestimated by Fourier techniques, as the amplitudes of peaks in the Fourier transform are based on the assumption of ideally periodic signal components. In this proof of concept work, a clear reduction in the observed peaks in the Fourier transform of the displacement error has been demonstrated, however, further work measuring the non-linearity errors directly in a more stable system, for example against an x-ray interferometer as in [4], is needed before the performance of the two-wavelength technique can be stated conclusively. For this reason, the term 'estimated residual non-linearity' is used throughout this work when discussing the achieved results.

The remainder of this discussion will be broken into sub-sections focussing on several key aspects of the two-wavelength non-linearity correction. First, experimental considerations that are not explored in this proof of concept work will be discussed. Following this, the existing limitations of, and potential improvements to, the proposed processing algorithm will be considered. A qualitative discussion of uncertainty contributions will then be made. Finally, potential avenues for further work will be proposed.

5.1. Experimental considerations

Several aspects of the two-wavelength correction methodology are sensitive to experimental conditions that are not explored in this work. Firstly the choice of λ_a and λ_b must be considered. In this case a HeNe laser operating at 633 nm was selected for λ_a due to the widespread use of this wavelength for metrological applications. The choice of λ_b was primarily determined by equipment availability, however it is anticipated that in practice a lower unstabilised laser is likely to be employed as the second wavelength, for example a diode laser, or a HeNe lasing at a different wavelength. The use of unstabilised lasers is possible as exact knowledge of λ_b is not required as a result of the rescaling of the λ_b displacements based upon the λ_a displacements. Several restrictions are placed on λ_b and the associated laser source. Any non-linearity harmonics present in the interferometer must not overlap between the two wavelengths, with the acceptable frequency spacing between harmonics determined by the frequency resolution of the displacement difference DFT (and therefore the displacement range covered and spatial sampling rate), the wavelength stability of the source laser and the stability of the non-linearities themselves. As alluded to by the previous restriction, λ_b must remain sufficiently stable for the duration of the measurement such that non-linearity harmonics can be separated in the DFT, with the required stability determined by the duration of the measurement, the non-linearity harmonics present in the interferometer, and the spacing of the wavelength harmonics. The λ_b source laser must also have a sufficient coherence length to cover the desired measurement range. In addition to these more fundamental restrictions, further restrictions may be imposed on λ_b if λ_a and λ_b are to be fibre coupled, due to the finite single mode wavelength range of commonly available optical fibres, necessitating the use of more expensive photonic-crystal fibres if the spacing between λ_a and λ_b is large. If both wavelengths are to be detected by the same detector, as is the case in this work, the availability detectors suitable for operation at both λ_a and λ_b must also be considered.

Along with the stability of the laser wavelengths, the stability of the non-linearities themselves may affect the correction. Residual non-linearities after applying a Heydemann style correction are likely to be higher order effects, existing due to unwanted cavity formation within the interferometer optics, with the cavity necessarily including a reflection from the moving mirror or retro-reflector for a non-linearity to be produced. As such the non-linearities targeted with

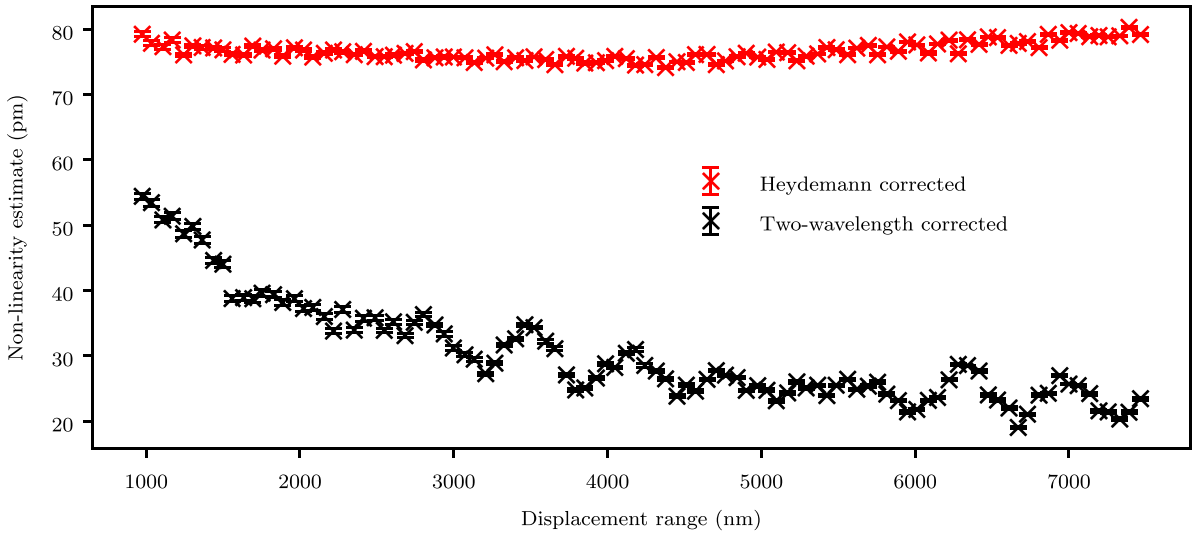

Figure 5. Variation of the non-linearity amplitude, estimated from the sum of the displacement error DFT peaks for the first three even harmonics, with displacement range.

the two-wavelength correction may be highly sensitive to the alignment of the interferometer optics with respect to the moving mirror or retro-reflector, an alignment that is prone to vary with both displacement and time. Variation in the amplitudes of the non-linearity harmonics manifests as broadened or split DFT peaks, and as such a wider frequency domain window will be required, again placing limits on the frequency spacing of harmonics of λ_a and λ_b in systems where non-linearities are prone to drift.

In this work combination and separation of the two wavelengths was achieved by multiplexing the fibre coupled laser sources together with a fibre switch at a relatively low switching frequency of 30 Hz. This approach, whilst adequate as a proof of concept, severely limits the measurement speed of the system and increases the effect of mechanical vibrations at higher frequencies than the switching speed on the displacement difference signal due to aliasing effects. As such alternatives would be preferable in practical application. Several approaches are possible, including spatially separating the two interferometers, modulation and lock-in amplification at different frequencies for each wavelength, separation with dichroic beam splitters or diffraction gratings, and separation via orthogonal polarisation. Of these techniques, modulation and lock-in amplification would be particularly well suited to heterodyne interferometer designs as such a modulation is already present. Most heterodyne interferometer designs are however reliant upon polarising optics, and finding polarising optics with suitable performance at both wavelengths may prove restrictive. Spatially separating the two interferometers would allow use of often lower cost and higher performing monochromatic optical components in both heterodyne and homodyne interferometer designs, and Abbe and cosine errors introduced by small misalignments between the optical axes of the two interferometers would, over sufficiently small measurement ranges, be compensated for by the rescaling effect of equation (11). Dichroic beam splitters offer a relatively straightforward implementation of the two-wavelength technique, however imperfect dichroic separation may result in the presence of λ_b harmonics in the λ_a displacement and visa versa. Leakage between the wavelengths of this sort would result in non-linearities common to both interferometers, which would not appear in the displacement difference and would therefore remain uncorrected. Leakage between the two wavelengths is also likely to prove problematic with diffraction grating or polarisation based separation.

A final experimental consideration is the required spatial sampling rate and displacement range. The minimum sampling rate is determined by the highest order non-linearity harmonic present in the interferometer, and as such will be highly dependant on the optical design of the interferometer. For the interferometer presented in this work higher order non-linearities are introduced by ghost reflections from the external surfaces of the PQBS cube and the stage mounted retro-reflector, and as such are attenuated by both the anti-reflection coating optics and by small misalignments between the optical surfaces. As such the highest order non-linearity observed occurs at a spatial period of approximately 105.5 nm ($\lambda_a/6$), requiring a spatial sampling period of 52.75 nm to resolve. Shorter wavelengths and the presence of higher order non-linearities will both serve to increase the required spatial sampling rate. The required displacement range for the correction to prove effective is related to the choice of wavelengths and spacing of the extant non-linearity harmonics as previously discussed, however as can be seen from figure 5 under the experimental conditions in this work, increased displacement range led to reduced residual non-linearities, with small increases in performance where the displacement range covered an integer number cycles of a non-linearity harmonic. This relationship may not hold true where non-linearities are highly variable with displacement, and in such cases over larger displacement ranges a moving overlapped DFT approach may prove preferable.

5.2. Data processing considerations

In addition to the experimental considerations, the performance of the correction may be sensitive to the data processing methods applied, in particular the displacement difference interpolation and tiling, and the frequency spacing windowing steps. Where the measured displacement profile is self overlapping, as is the case for both the mirrored linear and sinusoidal displacement profiles examined in this work, multiple displacement difference values exist at each measured displacement point. The effect of this on the interpolation process can be observed in figures 4(H and I) where peaks are present at short spatial periods due to the nearest neighbour interpolation algorithm switching between displacement differences measured at similar displacement values at differing time points. These short spatial period artefacts did not negatively affect the results as they occurred at spatial periods shorter than the highest order non-linearity harmonic present, and due to the highest resolved non-linearity harmonic being limited by the spatial sampling rate, this should remain the case in all systems. In this proof of concept experiment non-linearities are not the dominant uncertainty source, however, it should be noted that in practical application the two-wavelength correction is only beneficial in cases where the repeatability of the measurement is better than the Heydemann corrected non-linearities.

Both the choice of frequency space windowing function and frequency space window width have the potential to affect the correction process. In this work, possibly due to the relatively large amounts of both noise and drift present in the displacement measurements, the window function employed was not found to affect the residual non-linearities after correction, as such a simple rectangular window function was applied. In a more sensitive instrument, the ringing effects introduced by a rectangular frequency space window may become apparent, and alternative window functions may be required. The widths of the windows were found to strongly affect the results, with a window width determined in this work from the frequency resolution of the DFT. Increased window widths may be beneficial under some circumstances, for example where large variations in the non-linearities take place during the measurement process, leading to broadened DFT peaks.

5.3. Uncertainty

Uncertainties in the corrected displacements will be determined by the uncertainties in the displacement measurements at both wavelengths, and will in general be increased relative to the uncorrected uncertainty to a degree determined by the width of the frequency space window function. Non-linearities that vary with displacement, or wavelengths that vary over the course of the measurement will therefore increase the uncertainty in the corrected result due to the requirement for wider window functions. The frequency space windowing process will also introduce a degree of statistical correlation between individual corrected displacement measurements, and this may need to be considered if the corrected displacement values are to be further processed.

An additional uncertainty contribution arises from the fact that the displacement difference is sampled on a displacement basis that is itself non-linear, and this effect limits the ultimate performance of the correction. For the typically sub-nanometre non-linearity values encountered in precision displacement measuring interferometry, the effects of this 'timebase' modulation will be small. Higher order non-linearities will have a stronger timebase modulation effect as the ratio of the amplitude to the period of the distortion is increased, all else being equal.

Uncertainties in the values of the two wavelengths will also have an effect on the measurement uncertainty, with contributions arising from both uncertainty in the laser frequency, and uncertainty in the refractive index in the beam path. The λ_b wavelength is not used in the correction as implemented here, with the λ_b displacement scaled relative to the λ_a displacements, with the effective uncertainty in the average value of λ_b over the course of the measurement therefore determined by the uncertainty in the interferometric phase measurements made at λ_b (which are not affected by wavelength), and the uncertainty in λ_a. λ_a uncertainties in this case were dominated by the uncertainty in the refractive index as no Edlén correction was performed.

In this proof of concept work uncertainties in the measured displacements were dominated by longer period drift terms, rather than statistical uncertainties in individual measurement points or non-linearities, and as such a detailed assessment of the measurement uncertainty has not been made here.

5.4. Further work

As previously discussed, the Fourier technique employed in this work to estimate residual non-linearities has the potential to underestimate the residual non-linearity. As such, before the two-wavelength correction can be employed in rigorous metrological applications, a more accurate assessment of the residual non-linearities should be made. Direct traceable measurement of picometre scale non-linearities is possible through x-ray interferometry [3, 4].

In addition to verification of the performance of the correction, an uncertainty budget would be required for the displacement measurement in metrological applications. Uncertainties have not been assessed quantitatively in this work as it is clear from the results presented in figures 4(J–L) that non-linearities are not the dominant uncertainty source, and therefore any assessment of the uncertainty resulting from the two-wavelength correction could not be verified experimentally. Future work may develop an uncertainty budget, and this could again be verified with x-ray interferometry [4].

In addition to the reduction in residual non-linearities, two-wavelength interferometry also has to potential to allow for improved refractive index compensation [27], and this may be an avenue for future work. Further work may also investigate the application of the Fourier algorithm developed here to other differently non-linear *b* displacement measures, for example capacitive sensors as suggested in [26]. Conversely, the harmonic fitting approach proposed in [26] could be applied to two-wavelength interferometry, and may prove

preferable to the Fourier approach in cases where noise levels are low and non-linearities are stable with respect to both displacement and time over the ranges covered.

6. Conclusions

The two-wavelength non-linearity correction methodology has been shown to be capable of correcting for residual non-linearity errors that remain after application of Heydemann style [16, 17] ellipse fitting corrections. Residual non-linearities after Heydemann correction may be caused by polarisation leakage or unwanted back reflections (ghost reflections) within the interferometer optics, and affect both homodyne [10] and heterodyne [5, 7, 9, 11] interferometers. The two-wavelength correction is not dependant on a particular interferometer detection regime, and as such is anticipated to be applicable to both homodyne and heterodyne designs. In the best case a reduction in estimated non-linearity from 84 to 11 pm as compared to Heydemann corrected displacements was demonstrated for a linear displacement profile. In the worst case this reduction was from 89 to 26 pm for a sinusoidal displacement profile. This work is intended as a proof of concept, and as such the results presented here are not anticipated to represent the performance limits of the two-wavelength technique. Equally, as this is a proof of concept, further work is needed to quantify the uncertainties associated with the two-wavelength technique.

The proposed correction is implemented in post processing, and future work may implement the two-wavelength correction in a pseudo-real time manor, with rolling overlapping Fourier transforms. Additional future work could combine the two-wavelength non-linearity correction with two-wavelength refractive index compensation [27].

Data availability statement

The data that support the findings of this study are openly available at the following URL/DOI: 10.17862/cranfield.rd.14381993.

Acknowledgment

The authors thank Queensgate Instruments for the loan of the Queensgate Instruments NPS-X15A nanopositioning stage used to gather the experimental data presented in this work.

Funding

Engineering and Physical Sciences Research Council Industrial CASE studentship EP/R511894/1 (Project No. 2199 198); National Measurement System Engineering Measurement Programme, funded by the UK government Department for Business, Energy and Industrial Strategy; Royal Academy of Engineering Research Fellowship RF/201718/1745.

ORCID iDs

Angus Bridges https://orcid.org/0000-0002-5861-043X
Andrew Yacoot https://orcid.org/0000-0001-6740-821X
Thomas Kissinger https://orcid.org/0000-0003-1832-7143
David A Humphreys https://orcid.org/0000-0001-7720-6742
Ralph P Tatam https://orcid.org/0000-0001-9599-3639

References

[1] Peggs G N and Yacoot A 2002 A review of recent work in sub-nanometre displacement measurement using optical and X-ray interferometry *Philosophical Trans. Royal Society A* **360** 953–68
[2] Kang H J, Chun B J, Jang Y S, Kim Y J and Kim S W 2015 Real-time compensation of the refractive index of air in distance measurement *Opt. Express* **23** 26377–85
[3] Yacoot A, Bosse H and Dixson R 2020 The lattice parameter of silicon: a secondary realisation of the metre *Meas. Sci. Technol.* **31** 121001
[4] Pisani M *et al* 2012 Comparison of the performance of the next generation of optical interferometers *Metrologia* **49** 455–67
[5] Wu C M, Lawall J and Deslattes R D 1999 Heterodyne interferometer with subatomic periodic nonlinearity *Appl. Opt.* **38** 4089–94
[6] Fujimoto H, Mana G and Nakayama K 2000 Light bounces in two-beam scanning laser interferometers *Japan. J. Appl. Phys.* **39** 2870–5
[7] Wu C M 2002 Periodic nonlinearity resulting from ghost reflections in heterodyne interferometry *Opt. Commun.* **215** 17–23
[8] Cavagnero G, Mana G and Massa E 2005 Effect of recycled light in two-beam interferometry *Rev. Sci. Instrum.* **76** 053106
[9] Joo K N, Ellis J D, Spronck J W, van Kan P J M and Munnig Schmidt R H 2009 Simple heterodyne laser interferometer with subnanometer periodic errors *Opt. Lett.* **34** 386–8
[10] Hu P, Wang Y, Fu H, Zhu J and Tan J 2017 Nonlinearity error in homodyne interferometer caused by multi-order Doppler frequency shift ghost reflections *Opt. Express* **25** 3605–12
[11] Fu H, Wang Y, Hu P, Tan J and Fan Z 2018 Nonlinear errors resulting from ghost reflection and its coupling with optical mixing in heterodyne laser interferometers *Sensors* **18** 758
[12] Wu C M and Deslattes R D 1998 Analytical modeling of the periodic nonlinearity in heterodyne interferometry *Appl. Opt.* **37** 6696–700
[13] Bridges A, Yacoot A, Kissinger T and Tatam R P 2020 Polarization-sensitive transfer matrix modeling for displacement measuring interferometry *Appl. Opt.* **59** 7694–704
[14] Ahn J, Kim J A J W, Kang C S, Kim J A J W and Kim S 2009 A passive method to compensate nonlinearity in a homodyne interferometer *Opt. Express* **17** 23299–308
[15] Weichert C, Köchert P, Köning R, Flügge J, Andreas B, Kuetgens U and Yacoot A 2012 A heterodyne interferometer with periodic nonlinearities smaller than ±10 pm *Meas. Sci. Technol.* **23** 094005
[16] Heydemann P L M 1981 Determination and correction of quadrature fringe measurement errors in interferometers *Appl. Opt.* **20** 3382–4
[17] Birch K P 1990 Optical fringe subdivision with nanometric accuracy *Precis. Eng.* **12** 195–8
[18] Eom T B, Choi T Y, Lee K H, Choi H S and Lee S K 2002 A simple method for the compensation of the nonlinearity in the heterodyne interferometer *Meas. Sci. Technol.* **13** 222–5

[19] Požar T and Možina J 2011 Enhanced ellipse fitting in a two-detector homodyne quadrature laser interferometer *Meas. Sci. Technol.* **22** 085301
[20] Köning R, Wimmer G and Witkovský V 2014 Ellipse fitting by nonlinear constraints to demodulate quadrature homodyne interferometer signals and to determine the statistical uncertainty of the interferometric phase *Meas. Sci. Technol.* **25** 115001
[21] Watkins L R and Collet M J 2014 Ellipse fitting for interferometry. Part 2: experimental realization *Appl. Opt.* **53** 7697–703
[22] Collett M J and Tee G J 2014 Ellipse fitting for interferometry. Part 1: static methods *J. Opt. Soc. Am.* A **31** 2573–83
[23] Collett M J and Watkins L R 2015 Ellipse fitting for interferometry. Part 3: dynamic method *J. Opt. Soc. Am.* A **32** 491–6
[24] Hu P, Zhu J, Guo X and Tan J 2015 Compensation for the variable cyclic error in homodyne laser interferometers *Sensors* **15** 3090–106
[25] Kim J W J A, Kang C S, Eom T B and Ahn J 2009 A digital signal processing module for real-time compensation of nonlinearity in a homodyne interferometer using a field-programmable gate array *Meas. Sci. Technol.* **20** 017003
[26] Seppä J, Korpelainen V, Merimaa M, Picotto G B and Lassila A 2011 A method for linearization of a laser interferometer down to the picometre level with a capacitive sensor *Meas. Sci. Technol.* **22** 094027
[27] Meiners-Hagen K and Abou-Zeid A 2008 Refractive index determination in length measurement by two-colour interferometry *Meas. Sci. Technol.* **19** 084004
[28] Wu H, Zhang F, Liu T, Li J and Qu X 2016 Absolute distance measurement with correction of air refractive index by using two-color dispersive interferometry *Opt. Express* **24** 24361
[29] Liu Z, Li W, Bayanheshig Li X, Jiang S, Song Y and Lv Q 2017 Two-color heterodyne laser interferometry for long-distance stage measurement with correction of uncertainties in measured optical distances *Sci. Rep.* **7** 8173
[30] Meiners-Hagen K, Schödel R, Pollinger F and Abou-Zeid A 2009 Multi-wavelength interferometry for length measurements using diode lasers *Meas. Sci. Rev.* **9** 16–26
[31] Křen P and Balling P 2009 Common path two-wavelength homodyne counting interferometer development *Meas. Sci. Technol.* **20** 084009
[32] Raine K W and Downs M J 1978 Beam-splitter coatings for producing phase quadrature interferometer outputs *Opt. Acta* **25** 549–58
[33] Edlén B 1953 The dispersion of standard air *J. Opt. Soc. Am.* **43** 339–44
[34] Stone J, Phillips S and Mandolfo G 1996 Corrections for wavelength variations in precision interferometric displacement measurements *J. Res. Natl Inst. Stand. Technol.* **101** 671–4

2021-08-31

Correction of periodic displacement non-linearities by two-wavelength interferometry

Bridges, Angus

IOP

Bridges A, Yacoot A, Kissinger T, et al., (2021) Correction of periodic displacement non-linearities by two-wavelength interferometry. Measurement Science and Technology, Volume 32, Issue 12, December 2021, Article number 125202

https://doi.org/10.1088/1361-6501/ac1dfa